Journal of Applied Fluid Mechanics, Vol. 11, No. 6, pp. 1477-1488, 2018.
Available online at www.jafmonline.net, ISSN 1735-3572, EISSN 1735-3645.
DOI: 10.18869/acadpub.jafm.73.249.29036

Scale-Adaptive Simulation of Flow around a Circular Cylinder near a Plane Boundary

M. Grioni[1,2†], S. A. Elaskar[1,3] and A. E. Mirasso[2]

[1] *National Scientific and Technical Research Council, CONICET, Argentina*
[2] *Institute of Structural Mechanics and Seismic Risk, National University of Cuyo, Mendoza, 5500, Argentina*
[3] *Department of Aeronautical, National University of Córdoba, Córdoba, 5000, Argentina*

†*Corresponding Author Email: maurogrioni15@gmail.com*

(Received March 23, 2018; accepted June 19, 2018)

ABSTRACT

Numerical investigations using Scale-Adaptive Simulation (SAS) turbulence model are carried out to study the flow around a circular cylinder near to a plane boundary at Reynolds numbers between $8.6\text{x}10^4$ and $2.77\text{x}10^5$ with two different boundary layer thickness (δ) on the plane. The effects of gap (G) between the cylinder and the plane, the Reynolds number and the thickness of the plane boundary layer are analyzed through the drag and the lift coefficients, the Strouhal number, as well as through the wake flow structures behind the cylinder. Two and three-dimensional simulations are performed to examine the significance of the flow three-dimensionality when the cylinder is located near a plane. The SAS model results are compared with published experimental data and numerical results for similar flow conditions. The characteristics of the wake structures and force acting on the cylinder are in good agreement with previous studies. In general, the 3D-SAS model performed better than 2D-SAS. Based on the numerical results here obtained, the SAS turbulence model can be applied to study this flow configuration.

Keywords: SAS turbulence model; Circular cylinder; Vortex shedding; Boundary layers.

NOMENCLATURE

C_D	drag coefficient	U_∞	free-stream velocity
C_L	lift coefficient	U_δ	velocity outside the boundary layer
CFL	Courant–Friedrichs–Lewy number	x, y, z	cartesian coordinates
D	cylinder diameter	y^+	dimensionless wall distance
f	frequency	Δt	time step
G	gap between cylinder and plane	Δx	size of control volume
G/D_{crit}	critical gap ratio	α	power law exponent
Re	Reynolds number	δ	boundary layer thickness
RMS	root mean square	θ_s	separation angles
St	Strouhal number	μ	dynamic viscosity
t	time	ρ	density

1. INTRODUCTION

Flow past a circular cylinder is an active research topic of several disciplines due to its simple geometry and its great importance in several engineering applications. A particular characteristic of this flow is that the wake behind the cylinder is frequently associated with unsteady and periodic vortex shedding which causes dynamic forces on the structure. When a cylinder is placed near to plane wall, the wall proximity introduces additional complexity to the flow with patterns respect to an isolated cylinder. This flow mainly depends on three parameters: the Reynolds number (Re), the boundary layer thickness (δ), and the gap ratio (G/D), where G is the distance between the cylinder and the wall, and D is the cylinder diameter. In this paper, the flow around a cylinder close to a plane boundary is numerically studied because this phenomenon is present in many engineering problems encountered in heat exchangers, wind loads on storage horizontal tanks, submarine pipelines, etc.

During the last decades, a large numbers of experimental studies have been conducted on a circular cylinder near to a plane boundary, e.g. by Bearman and Zdravkovich (1978); Taniguchi and Miyakoshi (1990); Buresti and Lanciotti (1992); Lei *et al*. (1999); and Nishino *et al*. (2007). Most of the previous experiments were carried out in the range of Reynolds numbers $3x10^2$<Re<$1.4x10^5$, which correspond to subcritical flow regime for an isolated circular cylinder (Niemann and Holscher, 1990). On the other hand, Buresti and Lanciotti (1992) carried out experiments in upper subcritical and critical regimes. These studies have shown that the forces acting on the cylinder strongly depend on the distance between the cylinder and the wall (the gap G), and the suppression of vortex shedding appears when the gap, G, is below a critical distance. On the other hand, several numerical studies have been performed for flows around a circular cylinder near a plane wall. However, few of them were performed for high Reynolds number flows (Re>10^4). Lei *et al*. (2000) investigated the suppression of the vortex shedding by solving the Navier–Stokes equations and the Poisson equation for pressure in two-dimensional (2D) and time-dependent viscous flow using a finite difference method for Re from 80 to 1000. They showed that critical gap ratio (G/D_{crit}), at which the vortex shedding is suppressed, depends on Re: the critical gap ratio decreases as the Reynolds number increases. Dipankar and Sengupta (2005) solved the Navier–Stokes equations using 2D stream-function/vorticity formulation at Re=1200 and for G/D=0.5 and 1.5. Their computed results for lift and drag coefficients and the vortex shedding behavior were compared with experimental results. Ong *et al*. (2008) used the 2D Unsteady Reynolds-Averaged Navier Stokes (URANS) equations with the standard high Reynolds number *k*-*ε* model at Re ranging from $1x10^4$ to $4.8x10^4$ with δ/D=0.14-2. They found that under-prediction of the hydrodynamic quantities (C_D, C_L, St and C_P) is observed in the subcritical flow regime due to limited capacity of the k–ε model to predict accurately the flow around the cylinder. Nishino *et al.* (2008) used URANS simulation and Detached-Eddy Simulation (DES) to simulate the flow around a circular cylinder placed near to a moving wall at Re=$4x10^4$. In Deepakkumar *et al.* 2017, two dimensional flow past circular cylinder confined by walls with local waviness near the cylinder has been studied by assuming that the flow is laminar flow at Re=200. Although different simulation techniques with diverse turbulence models have been considered before, it is today a challenging subject of computational fluid dynamics (CFD) to reproduce with sufficient accuracy the flow separation and the wake structures behind a cylinder near a plane boundary.

Direct Numerical Simulation (DNS) is believed to be capable of giving better results; however, this type of simulation is not currently feasible because of too high computational costs required. Other option is to apply Large Eddy Simulation (LES), but the use of LES still requires large computational resources for the resolution of the near-wall region, especially in high Re flows. A possible alternative to LES is the hybrid model DES, such as used by Nishino *et al.* (2008) mentioned before, which solves standard RANS equations in the attached boundary layer regions and switches to a LES model for detached flow regions. This approach has shown promising results for several technical flows (Shur *et al*, 2002), but the switch between LES and RANS mode depends on the local mesh spacing and can lead to a premature mesh-induced separation in the attached boundary layer. As an alternative to remedy this problem, Menter *et al.* (2003) proposed a so-called Scale-Adaptive Simulation (SAS) model. This model provides standard RANS capabilities in stable flow regions and it can switch to LES-like mode in unsteady regions of the flow field, but without the explicit mesh dependence in the RANS regime. In this study the SAS is combined with SST (Shear Stress Transport) and it can be found implemented in Ansys Fluent software. As far as we know, no studies have implemented the SAS model to simulate the flow around a cylinder near a plane boundary.

Taking into account the SAS capabilities to capture turbulent structures and the fact that there are very few experimental and numerical studies of circular cylinder near a plane wall for Re>10^4, the main objective of the present study is to evaluate whether, and how accurately, the SAS model can reproduce the vortex shedding and the forces acting on the cylinder when it is located near to a wall at Re in upper subcritical and critical flow regime. Numerical simulations are carried out in both two and three-dimensional domains at Re=$8.6x10^4$, $1.89x10^5$ and $2.77x10^5$ with two different boundary layer thicknesses δ/D=0.1 and 1.1. It is expected that this study would provide further insight into the mechanisms of the flow and force variations for the problem of a cylinder near a plane boundary.

2. COMPUTATIONAL MODELING

2.1 Flow Equations and SAS Turbulence Model

This section describes the used equations in the modeling and also explains the adopted turbulence modeling approach. The equations to be solved are the incompressible Reynolds-averaged equations for conservation of mass and momentum, given by

$$\frac{\partial(\rho U_i)}{\partial x_i} = 0 \tag{1}$$

$$\frac{\partial(\rho U_i)}{\partial t} + \frac{\partial(\rho U_i U_j)}{\partial x_j} = -\frac{\partial P}{\partial x_i} + \frac{\partial}{\partial x_j}\left[\mu\left(\frac{\partial U_i}{\partial x_j} + \frac{\partial U_j}{\partial x_i}\right) - \rho\overline{u_i' u_j'}\right] \tag{2}$$

where ρ is the density of the fluid, t is the time, U_i is the average component of the velocity in the

direction x_i, P is the mean pressure, μ is the dynamic viscosity and u' is the fluctuating component of velocity.

As a result of Reynolds-averaging, additional terms are introduced into the momentum equations. These terms are called Reynolds stresses and must be modeled in order to close the system of equations. The Boussinesq hypothesis state that the Reynolds stresses is proportional to the mean strain rate:

$$\tau_{ij} = -\rho\overline{u_i' u_j'} = \mu_t\left(\frac{\partial U_i}{\partial x_j} + \frac{\partial U_j}{\partial x_i}\right) - \frac{2}{3}\rho k \delta_{ij} \quad (3)$$

where μ_t is the turbulent viscosity, k is the turbulence kinetic energy and δ_{ij} is the Kronecker delta.

The SST model was proposed by Menter (1994) to combine the best characteristics of the k-ω and k-ε models, and also to lead to major improvements in the prediction of adverse pressure gradient flows. The values of k and ω are directly obtained from the turbulent kinetic energy (k) and turbulence eddy frequency (ω) transport equations, which are given by Eqs. (4) and (5), respectively:

$$\frac{\partial(\rho k)}{\partial t} + \frac{\partial}{\partial x_j}\left(\rho U_j k\right) = \frac{\partial}{\partial x_j}\left[\left(\mu + \sigma_{k3}\mu_t\right)\frac{\partial k}{\partial x_j}\right] + P_k - \rho\beta' k\omega \quad (4)$$

$$\frac{\partial(\rho\omega)}{\partial t} + \frac{\partial}{\partial x_j}\left(\rho U_j \omega\right) = \frac{\partial}{\partial x_j}\left[\left(\mu + \sigma_{\omega 3}\mu_t\right)\frac{\partial \omega}{\partial x_j}\right] + \alpha_3 \frac{\omega}{k}\tau_{ij}\frac{\partial U_i}{\partial x_j} - \rho\beta_3\omega^2 + 2\rho\left(1 - F_1\right)\sigma_{\omega 2}\frac{1}{\omega}\frac{\partial k}{\partial x_j}\frac{\partial \omega}{\partial x_j} \quad (5)$$

The turbulence viscosity is calculated as,

$$\mu_t = \frac{\alpha_1 k\omega}{\max\left(\alpha_1\omega, SF_2\right)} \quad (6)$$

where the constants employed in the SST models are, β'=0.09; $\sigma_{\omega,2}$=0.856; α_1=0.31 and S is the strain rate magnitude. F_1 and F_2 are blending functions, based on wall distance, that switch smoothly between the two turbulence models. Constants with subscript 3 are blends between the constants in the k–ε and k–ω models (Menter, 1994). Although the SST model has shown a good performance near the wall region, in transient flows it has the drawback of producing too large turbulent length-scales. In the SAS approach, this limitation is overcomed by introducing the von Karman length-scale, which is given by,

$$L_{vK} = \kappa\sqrt{\left|\frac{\left(\frac{\partial U_i}{\partial x_j}\right)\left(\frac{\partial U_j}{\partial x_i}\right)}{\left(\frac{\partial^2 U_i}{\partial x^2{}_j}\right)\left(\frac{\partial^2 U_i}{\partial x^2{}_k}\right)}\right|} \quad (7)$$

where κ is the von Karman constant. The information provided by the von Karman length scale allows to preserve the SST model in steady regions and to activate the SAS capability in unsteady regions of the flow field.

The SAS model equations differ from those of the SST model by the additional SAS source term (Q_{SAS}) in the transport equation for the turbulence eddy frequency (Eq. (5)). Based on the SST model, SAS formulation can be presented by incorporating an additional source term (Q_{SAS}) in the transport equation for the turbulence eddy frequency (Eq. (5)).

$$Q_{SAS} = \max[\rho\xi_2\kappa S^2\left(\frac{L}{L_{vK}}\right)^2 - C\frac{2\rho k}{\sigma_\Phi}\max\left(\frac{1}{\omega}\frac{\partial\omega}{\partial x_j}\frac{\partial\omega}{\partial x_j}, \frac{1}{k^2}\frac{\partial k}{\partial x_j}\frac{\partial k}{\partial x_j}\right), 0] \quad (8)$$

where the model parameters are given as ξ_2=3.51; σ_Φ=2/3, and C=2. The turbulent length scale (L) derived from the SST model is given as,

$$L = \frac{\sqrt{k}}{c_\mu^{0.25}\omega} \quad (9)$$

Then, the turbulent eddy viscosity for the SAS model results:

$$\mu_t = \rho\cdot\left(\sqrt{((\beta_3/c_\mu) - \alpha_3)/(\kappa\eta_2)}\cdot L_{vK}\right)^2 S \quad (10)$$

2.2 Numerical Solver

The flow around a cylinder is simulated considering the influence of a wall plane by changing the gap ratio G/D from 0.2 to 1.5. The simulations are conducted using the commercial CFD code ANSYS Fluent 15 (Fluent Inc, 2014), in which a finite volume method is used to solve the governing equations for incompressible turbulent. A Semi-Implicit Method for Pressure Linked Equations algorithm (SIMPLE) is used for the velocity-pressure coupling. Second-order schemes are used for the discretization of pressure and turbulent quantities. The momentum equations are discretized with a bounded central differencing, while the unsteady formulation is based on a bounded second-order implicit scheme.

For all the simulations here performed, structured meshes are used to discretize the computational domain. A mesh convergence study has been carried out in order to examine the influence of spatial resolution on the results. More details about the mesh convergence are described later.

For most of the unsteady simulations in this study, 5-15 inner iterations per time step is found to be sufficient to achieve the convergence of the solution. The dimensionless time step $\Delta tU_\infty/D$ is set at 0.0093, which ensured a CFL number (CFL= $\Delta tU_\infty/\Delta x$) less than 2 for the entire computational domain. In order to ensure the time step convergence, a smaller step $\Delta tU_\infty/D$ of 0.0047 (CFL<1 for the entire computational domain) is used for comparison. Further details of the time step convergence are described below. The transient simulations are first run until the stationary periodic flow pattern is achieved, and are then further continued about 20-25 vortex-shedding cycles in order to obtain time-averaged data of the flow sufficiently long allowing a reliable analysis.

A schematic diagram of the computational domain and boundary conditions employed for the simulations in this work are shown in Fig. 1. Different steady inlet conditions with low turbulence level (turbulence intensity of 0.9% and unity turbulent viscosity ratio) are imposed, so that a specific velocity profile is achieved in the cylinder position. At the outlet, a condition of zero-diffusion-flux for all variables in the streamwise direction is applied. This condition is referred as the 'outflow' boundary condition in Fluent. For the upper boundary of the domain (Top), free-slip wall is specified. For the side boundaries, periodic conditions are imposed in the spanwise direction. No-slip condition is imposed on the cylinder surface and the bottom plane boundary (Ground), i.e the velocity at the wall is zero.

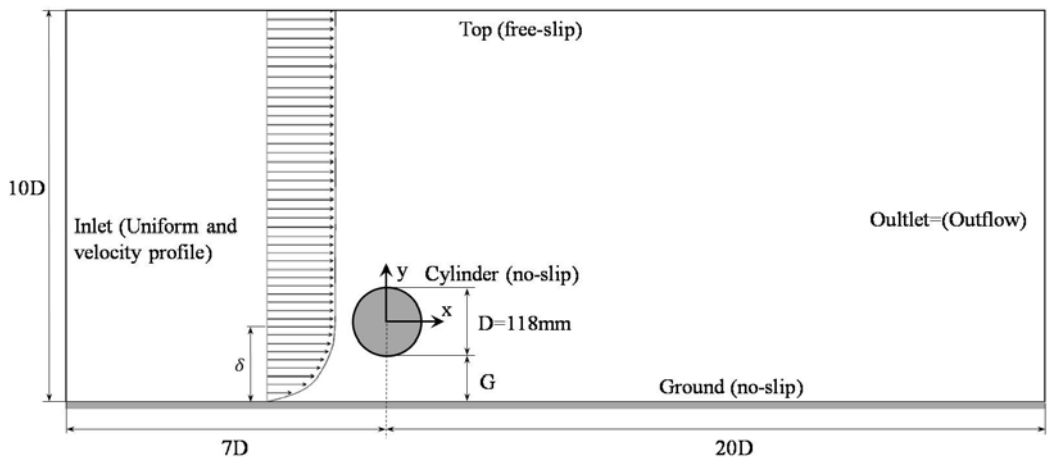

Fig. 1. Schematic diagram of the computational domain and boundary condition.

2.3 Boundary Layer Generation

In this study, two different boundary layer thicknesses (δ) on the plane boundary (ground) are considered for the simulation. These boundary layers, which correspond with those obtained experimentally in a wind tunnel by Buresti and Lanciotti (1992), are determined by measuring the velocity profile of the boundary layer at the cylinder location but with the cylinder removed (i.e. in the absence of the cylinder). To reproduce the experimental boundary layers, the following process is carried out. Keeping the same computational domain, the cylinder is removed and its space is filled with a mesh with the same resolution as the mesh in the vicinity of the wall. The mean streamwise velocity is sampled on several vertical cross-sections (see Fig. 2), from the inlet until the velocity profile correctly reproduces the boundary layers obtained experimentally by Buresti and Lanciotti (1992). The boundary layer 1 (BL1) is achieved in the cross-section corresponding to a distance of 7D from the inlet when a uniform flow is imposed at the inlet. While the boundary layer 2 (BL2) is attained again in the cross-section corresponding to a distance of 7D from the inlet but when a velocity distribution with a power law ($U=U_\delta(y/\delta)^\alpha$, where α denotes the exponent of the power law α=0.11 and U_δ is the velocity outside the boundary layer) is applied at the inlet. Comparison of the velocity profiles between the experimental and simulated boundary layers for the different velocities are shown in Figs. 3 and 4. The numerical and experimental boundary layers show good agreement.

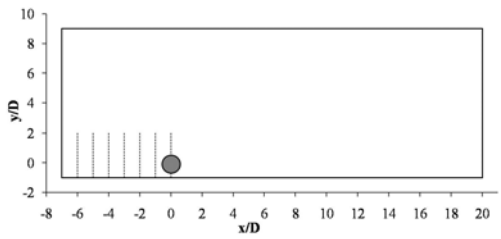

Fig. 2. Representation of the sampling vertical cross-section indicated with dotted lines.

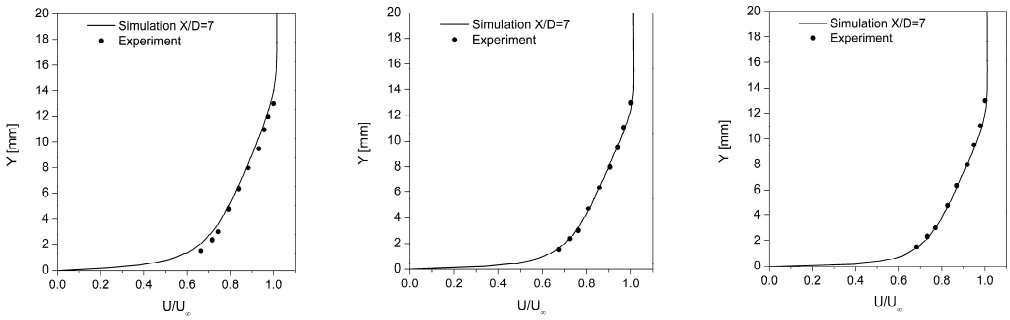

Fig. 3. Normalized velocity profile (U/U_∞) for the boundary layer 1 (δ/D=0.1): a) Re=8.6x10^4, b) Re=1.89x10^5 y c) Re=2.77x10^5.

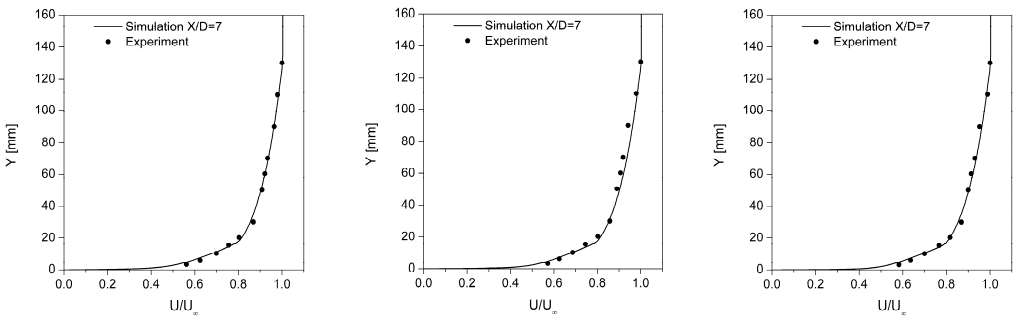

Fig. 4. Normalized velocity profile (U/U_∞) for the boundary layer 2 (δ/D=1.1): a) Re=8.6x10^4, b) Re=1.89x10^5 y c) Re=2.77x10^5.

2.4 Computational Mesh

Two and three-dimensional multi-block structured meshes are created with ANSYS ICEM CFD (Ansys ICEM, 2014) to be used with SAS turbulence model. The mesh resolution over the cylinder is similar to the mesh used for a circular cylinder in free stream by Menter *et al.* (2003) to show the capability of SAS model to capture the turbulence structures. An example of the two-dimensional mesh is shown in Fig. 5 with a refinement near the cylinder and the ground. The distance from the cylinder and ground surfaces to the nearest mesh points is chosen such that the dimensionless wall distance y^+ is kept below 1. For the two-dimensional (*x*-*y*) meshes, 160 mesh points are equidistantly located around the cylinder resulting in a total mesh of 27219 hexahedral elements for all related G/D. The three-dimensional meshes are obtained simply extending the two-dimensional mesh in the spanwise (*z*) direction. The domain spanwise extension is set at 2 diameters (D), which is certainly the lowest limit acceptable for turbulence resolving models (Menter *et al*, 2003), with 20 elements equidistantly located in the *z* direction. In this way, the three-dimensional mesh consists of 544380 hexahedral elements.

In order to investigate the effect of the proximity of a cylinder to the ground, 10 different meshes are created, one for each G/D ratio=0.2, 0.3, 0.4, 0.8 and 1.5, and for both the two and three-dimensional cases. As the cylinder moves away from the ground, the number of mesh points between the cylinder and the ground is increased, and decreased between the cylinder and the top of the domain. This distribution is defined in order to keep similar mesh aspect ratio but without changing the number of points in the *y* direction. In addition to these 10 meshes for the main part of the study, other four meshes are built to examine the dependency of the results with the mesh.

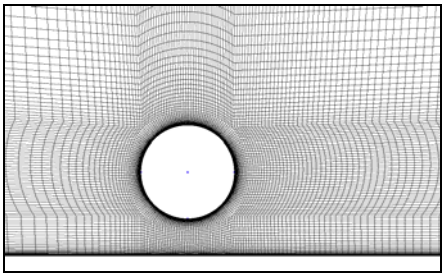

Fig. 5. Example of computational mesh near the cylinder for G/D=0.4.

2.5 Convergence Studies

The mesh and time step convergence study is performed for the flow at Re=8.6x10^4 and for G/D=0.4 with 4 meshes of different spatial resolutions (in the *x*-*y* plane and also in the *z* direction) and two different time resolutions as summarized in Table 1. To analyze the numerical results, the mean drag and lift coefficients and Strouhal number values are compared for this study. The case defined as "baseline" in the Table 1 indicates the adopted spatial and time resolution in present study.

A comparison of the influence of spatial resolution in the *x* and *y* directions with 20 elements in *z*

Table 1 Time average values of C_D, C_L and St with different Spatial and time resolution (Re=8.6x10^4, G/D=0.4).

Case	Mesh (x, y)	Mesh (z)	ΔtU_∞/D	C_D	C_L	St
3D-SAS (Baseline)	27219	20	0.0093	1.039	0.168	0.250
Resolution (x,y)						
M1	13839	20	0.0093	1.004	0.176	0.264
M2 (=Baseline)	27219	20	0.0093	1.039	0.168	0.250
M3	55683	20	0.0093	1.019	0.165	0.262
Resolution (z)						
M4	27219	10	0.0093	1.062	0.183	0.250
M5 (=Baseline)	27219	20	0.0093	1.039	0.168	0.250
M6	27219	40	0.0093	1.038	0.168	0.275
Resolution in time						
T1 (=Baseline)	27219	20	0.0093	1.039	0.168	0.250
T2	27219	20	0.0047	1.020	0.181	0.255

direction are shown for the cases M1, M2 (=Baseline) and M3. In order to obtain a constant mesh refinement ratio, in case M1 the number of mesh points in each (x and y) direction is determined in such a way that the baseline results in 50% more points than the M1 mesh. Whereas in case M3, the number of mesh points is increased by 50% from the baseline. It can be seen from the results that the convergence is not so clear. However, the difference between cases M2 and M3 is smaller than those between cases M1 and M2, suggesting a certain degree of mesh convergence in the x and y directions.

In addition, cases M4, M5 (baseline) and M6 with 10, 20 and 40 elements in the spanwise direction, respectively, show the influence of mesh resolution in the z direction. Accordingly, this study shows that a good degree of mesh convergence is achieved.

In order to ensure the time step convergence, the case T1 (baseline) and T2 are compared. In case T2, the time step is reduced to half of T1, resulting in a Courant number of CFL<1. The differences in the obtained results between the cases T1 and T2 are found to be small, as shown in Table 1.

3. RESULTS AND DISCUSSION

Numerical simulations are carried out at Reynolds numbers from 8.6x10^4 to 2.77x10^5 with two different types of boundary layers on the ground, having relative thicknesses δ/D from 0.1 to 1.1, and for gap ratios G/D=0.2, 0.3, 0.4, 0.8 and 1.5. Two types of simulations are performed in this study, referred to as "2D-SAS" and "3D-SAS" using two and three-dimensional meshes, respectively. A summary of the computational conditions are shown in Table 2.

3.1 Force Coefficients and Strouhal Number

The overall features of the flow are represented by the drag and lift coefficients and the Strouhal number. The drag (C_D) and lift (C_L) coefficients are defined as: C_D=F$_D$/(0.5ρU_∞^2A) where F$_D$ is the drag force exerted on the cylinder, and A is the projected area of the cylinder; C_L= C_L=F$_L$/(0.5ρU_∞^2A), where F$_L$ is the lift force exerted on the cylinder. The Strouhal number is defined as St=fD/U_∞, where f is the vortex shedding frequency obtained from the fluctuating lift force. Figures 6 and 7 compare the time averaged drag and lift coefficients, respectively, computed over the cylinder for different gap ratios G/D with the experimental data by Buresti and Lanciotti (1992). As can be seen from the figures, predicted behavior of the drag and lift by the 2D and 3D-SAS simulations are in good agreement with experimental data. In fact, C_L values show a better accuracy regarding the experimental values. Meanwhile, the drag behavior shows a slightly larger difference with the experiments.

Considering the drag coefficient, the numerical results from 2D-SAS are in agreement with the experiments for the lowest Re (Re=8.6x10^4, subcritical regime), while 3D-SAS results show good correlation with experimental values for the highest Re (Re=2.77x10^5, critical regime). For intermediate Re (Re=1.89x10^5) both 2D-SAS and 3D-SAS show a slightly difference with experimental data. It should be noted, that the 3D-SAS has the drawback of the lack of accurate results (under-predict the C_D values) when the cylinder is far from the wall plane (G/D>0.8) for lower Re, especially for Re=8.6x10^4 (subcritical regime). It can be explained by the angle where the flow separation occurs, measured from the front position of the cylinder to the separation position. The flow behavior for this Re (Re=8.6x10^4 subcritical regime) is characterized by a laminar separation at an angle of θ_S=70°-80° from the stagnation point (Achenbach 1971). For G/D=1.5, where the influence of the ground is negligible and consequently the pressure distribution becomes symmetric about the horizontal centerline of the cylinder, the 3D-SAS model predicts the separation point at an angle of 95° (Grioni, Elaskar and Mirasso; unpublished results), which would explain the reduction in the drag coefficient.

Table 2 Summary of the computational conditions.

Case	Type	G/D	δ/D	Re
2D	2D-SAS	0.2, 0.3, 0.4, 0.8 ,1.5	0.1 , 1.1	$8.6\text{x}10^4$, $1.89\text{x}10^5$, $2.77\text{x}10^5$
3D	3D-SAS			

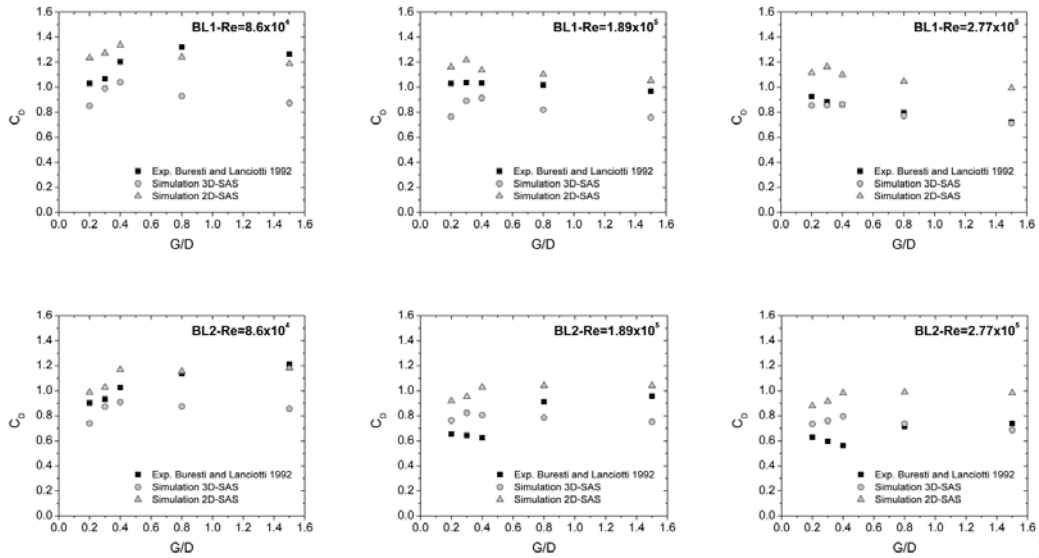

Fig. 6. Drag coefficient (C_D) versus gap to diameter ratio.

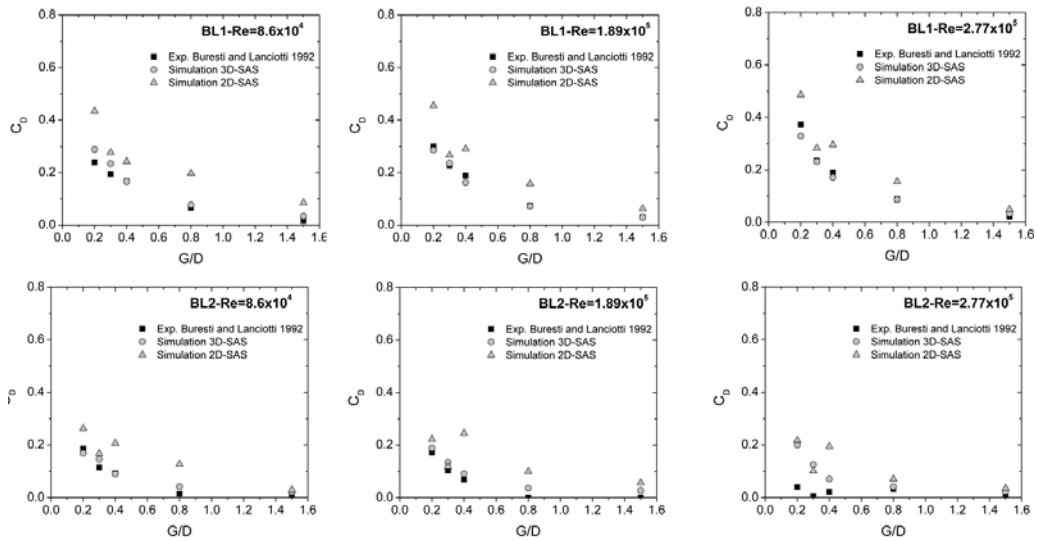

Fig. 7. Lift coefficient (C_L) versus gap to diameter ratio.

Considering the lift coefficient for all the cases, 3D-SAS shows a better agreement than 2D-SAS with the experimental study by Buresti and Lanciotti (1992). Despite 3D simulations properly capture the C_L decrease when the gap ratio G/D increases, the discrepancy for the case BL2-Re=$2.77\text{x}10^5$ between the simulations and experiments is not clear. However, a variation of C_L with the gap ratio G/D similar to the numerical results was reported by Göktun (1975), who investigated the flow around a circular cylinder near a wall at a Reynolds number of $2.5\text{x}10^5$.

In Fig. 8, the variation of the Strouhal number with the gap ratio at a Reynolds number of $8.6\text{x}10^4$ can be found. The results for 2D-SAS and 3D-SAS are compared with experimental results at the same Re from Buresti and Lanciotti (1992). It should be noted that both two and three-dimensional SAS show a similar behavior. While Strouhal numbers values computed are higher (overpredict) for all gap, G/D's, the same trend is observed when is compared with experimental data. Rajani *et al.* (2012), recently reported a similar overpredicted value (St≈0.25) at Re=$1\text{x}10^5$, for 2D URANS simulations of a circular cylinder in free-stream using three turbulence models, including the SST turbulence model. An interesting observation to note is that the Strouhal numbers obtained for 2D-SAS simulations are slightly higher than those calculated with 3D-SAS.

The Strouhal number St predicted by the 3D-SAS simulations for the Re numbers of $1.89\text{x}10^5$ and $2.77\text{x}10^5$ are shown in Fig. 9. As it is observed for Re=$8.6\text{x}10^4$, in Fig. 9 the Strouhal number St is almost independent of G/D, which is consistent with previously published results by Bearman and

Zdravkovich (1978), Taniguchi and Miyakoshi (1990), and Lei *et al.* (1999).

3.2 Vortex Shedding and Suppression

The vortex shedding flow behind a cylinder placed at various gap distances from the plane boundary is discussed by examining the time histories of the force coefficients (C_D, C_L) and vortex shedding flow structures, which are visualized through velocity field contours and the iso-surface of the Q-criterion. Also, the variation of the root-mean-square of the lift coefficient (C_{Lrms}) with the gap ratio is presented and compared with the experimental results by Buresti and Lanciotti (1992).

Figure 10 shows the time variations of the force coefficients of the cylinder as function of the nondimensional time, $=tU_\infty/D$, and a typical instantaneous contours of the velocity field in the mid-span sections, predicted by the 3D-SAS for different gap ratios at Re=8.6x10^4 with δ/D=0.1. The solid and dashed lines represent the variations of C_D and C_L, respectively. The velocity contour plots are included in these figures to highlight the flow structures.

By analyzing the results, three different flow regimes can easily observed as a function of G/D: (i) For large gap ratios (G/D>0.8), the influence of the wall can be neglected and the vortex shedding characteristic is similar to an isolated cylinder (i.e. stand-alone cylinder); (ii) For an intermediate gap ratios (0.3<G/D<0.8), the vortex shedding is still present and the effect of the wall boundary on the vortex shedding becomes considerable, causing an asymmetric flow (about x direction) behind the cylinder; (iii) For small gap ratios (G/D<0.3), the periodic vortex shedding is suppressed defining G/D=0.3 as a critical gap (G/D$_{crit}$). These regimes agrees with that reported in Wang and Tan (2008) on a circular cylinder using particle image velocimetry (PIV) for a Reynolds number Re=1.2x10^4 with an incident boundary layer thickness δ/D=0.4. Also, Nishino *et al.* (2007) and Nishino *et al.* (2008) have observed similar regimes in both their experimental and numerical results at comparable Reynolds numbers (Re=4x10^4 and 1x10^5) but no boundary layer was considered on the ground.

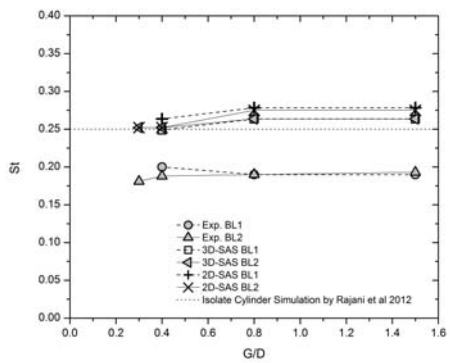

Fig. 8. Strouhal number versus gap to diameter ratio for Re=8.6x10^4.

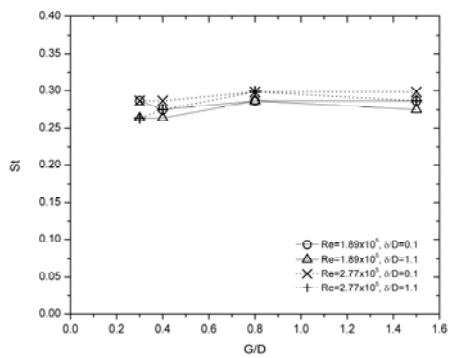

Fig. 9. Strouhal number versus gap to diameter ratio for Re=1.89x10^5 and 2.77x10^5 (3D-SAS).

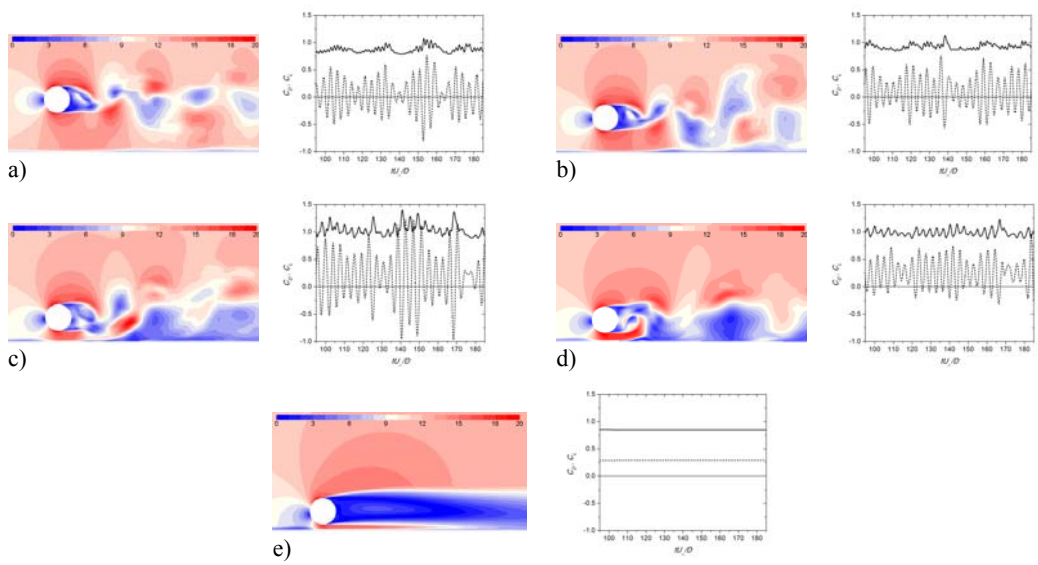

Fig. 10. 3D-SAS contours of the magnitude of instantaneous velocity (m/s) and time variation of C_D (solid line) and C_L (dashed line) for BL1 and Re=8.6x10^4; a) G/D=1.5; b) G/D=0.8; c) G/D=0.4; d) G/D=0.3; e) G/D=0.2.

Figure 11 shows the time variations of the force coefficients and a typical instantaneous contours of the velocity field provided by the 2D-SAS simulations for different gap ratios at Re=8.6x10^4 with δ/D=0.1. The solid and dashed lines represent the variations of C_D and C_L, respectively. It should be noted that, in contrast to the 3D-SAS, the time evolution of the lift coefficient predicted by 2D-SAS oscillates regularly and with a large amplitude even at G/D=0.2, where the vortex shedding is supposed to be suppressed according to the experiments. This phenomenon can also be seen in Fig. 11 by means of the contours of the velocity field. It is important to mention that additional computations are carried out at G/D=0.1 obtaining the cessation of vortex shedding for the 2D-SAS simulations. This reduction of the value of the critical gap ratio could be explained due to the large amplitude of the fluctuating lift predicted by 2D-SAS. It is inferred that larger amplitude of the fluctuating lift reveals a greater strength of vortex shedding behind a cylinder whereby the suppression of vortex shedding is more difficult to achieve resulting in a smaller G/D$_{crit}$.

A summary of the critical value for suppression of vortex shedding (G/D$_{crit}$) is given in Table 3 for the three Reynolds numbers and for the two boundary layers of the ground considered in the present study.

The critical gap predicted by both models (2D-SAS and 3D-SAS) are equal for Re=2.77x10^5; a difference appears for Re=1.89x10^5 and δ/D=0.1; whereas for Re=8.6x10^4 the results differ slightly for both boundary layer thicknesses. Taking into account the experimental values obtained by Buresti and Lanciotti (1992) for Re=8.6x10^4, 3D-SAS shows a better agreement than 2D-SAS.

By analyzing the effect of Reynolds number on vortex shedding suppression, it is observed from Table 3 that G/D$_{crit}$ predicted by 2D-SAS remains unchanged with the Re, while 3D-SAS shows that G/D$_{crit}$ decreases when Re increases, i.e., the critical distance of the cylinder to the ground for vortex shedding suppression decreases as the Reynolds number increases. Probably, this change in G/D$_{crit}$ with Re could be related to a change in the characteristic of the flow regimes (subcritical to critical) than with a change of the Reynolds number itself. Ong *et al.* (2010) found a similar relation between Re and G/D$_{crit}$ for 2D numerical simulation: G/D$_{crit}$=0.3 for Re=1.31x10^4 and G/D$_{crit}$≈0.1-0.15 for Re=3.6x10^6, both simulations with δ/D=0.48.

By considering the effect of boundary layer thickness (δ) on vortex shedding suppression, Buresti and Lanciotti (1992) found that the critical gap ratio (G/D$_{crit}$) is about 0.4 for the thin boundary layer (δ/D=0.1), whereas it decreases to about 0.3 for the thicker boundary layer (δ/D=1.1) at Re=8.6x10^4. These observations are in good agreement with those of Lei *et al.* (1999), who showed that vortex shedding is suppressed at a gap ratio of about 0.4-0.3, as the thickness of the boundary layer increases from δ/D=0.14 to δ/D=2.89 for Re=1.35x10^4. On the other hand, Taniguchi and Miyakoshi (1990) showed that G/D$_{crit}$ gradually increases with the increase of δ: from G/D$_{crit}$=0.3 for δ/D≈0.4 to G/D$_{crit}$=0.9 for δ/D≈1 at comparable Reynolds numbers (Re=9.4x10^4). The present numerical study indicates that the critical gap does not show a high dependency on the incident boundary layer thickness (δ), although for Re=1.89x10^5 the results obtained by the 3D-SAS show that G/D$_{crit}$ decreases from 0.3 to 0.2, as δ/D increases from 0.1 to 1.1, which is coincident with the trend observed by Buresti and Lanciotti (1992) and Lei *et al.* (1999).

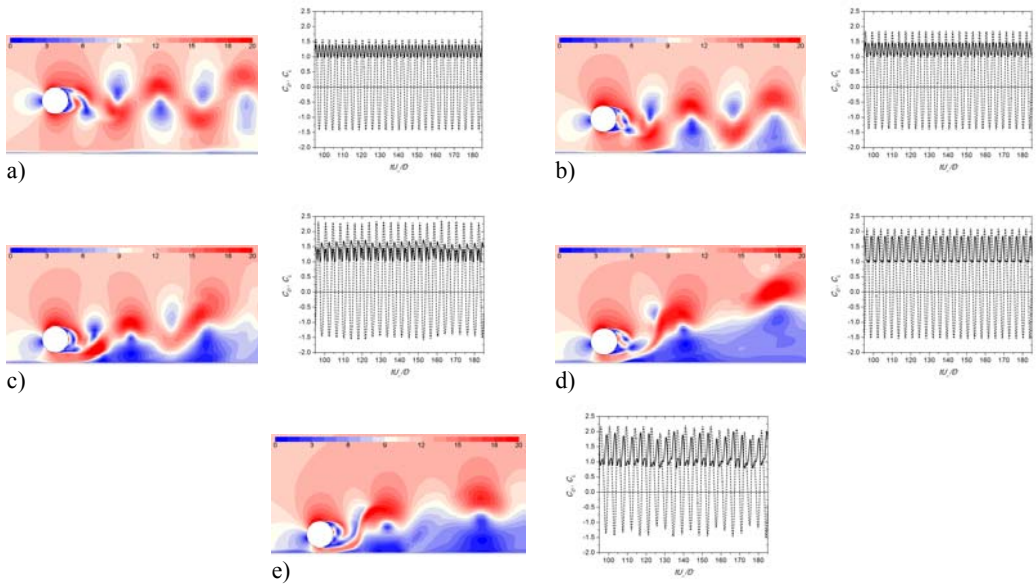

Fig. 11. 2D-SAS contours of the magnitude of instantaneous velocity (m/s) and time variation of C_D (solid line) and C_L (dashed line) for BL1 and Re=8.6x10^4; a) G/D=1.5; b) G/D=0.8; c) G/D=0.4; d) G/D=0.3; e) G/D=0.2.

Table 3 Summary of computational results for the suppression of vortex shedding.

Re	δ/D	G/D$_{crit}$ (2D-SAS)	G/D$_{crit}$ (3D-SAS)	G/D$_{crit}$ Buresti and Lanciotti 1992
8.6x10^4	0.1 1.1	0.2 0.2	0.3 0.3	0.4 0.3
1.89x10^5	0.1 1.1	0.2 0.2	0.3 0.2	- -
2.77x10^5	0.1 1.1	0.2 0.2	0.2 0.2	- -

The magnitude of the fluctuating lift coefficient can be represented by its root-mean-square (RMS) value, C_{Lrms}. Figure 12 presents the variations of C_{Lrms} with the gap ratio and Reynolds number predicted by the 2D and 3D-SAS simulations, with Fig.12a showing the values for the boundary layer thickness δ/D=0.1, and Fig. 12b showing the values for the boundary layer thickness δ/D=1.1. The results of the experiments conducted by Buresti and Lanciotti (1992) are also shown in the figure for comparison. The figures clearly show that the 2D simulations over-predict C_{Lrms} compared with the experimental data, whereas 3D simulations show a good agreement with the experimental results. Recently, Abrahamsen Prsic *et al.* (2016) showed a similar behavior for the 2D and 3D simulations using a LES model to study the flow around a cylinder placed at a distance of G/D=0.6 from the wall at Re=1.31x10^4.

Figure 13 shows instantaneous wake structures of the cylinder visualized with the use of iso-surfaces of the Q-criterion ($Q=1/2(\Omega^2-S^2)$; where S is the strain rate and Ω is the vorticity) colored with the turbulence viscosity ratio magnitude. It can be seen a clear difference in both cases G/D=0.8 and G/D=0.2. In Fig. 13a a three dimensional alternated vortex shedding are generated behind the cylinder at G/D=0.8, whereas in Fig. 13b two shear layers from both sides of the cylinder with a small turbulent structures can be identified at G/D=0.2.

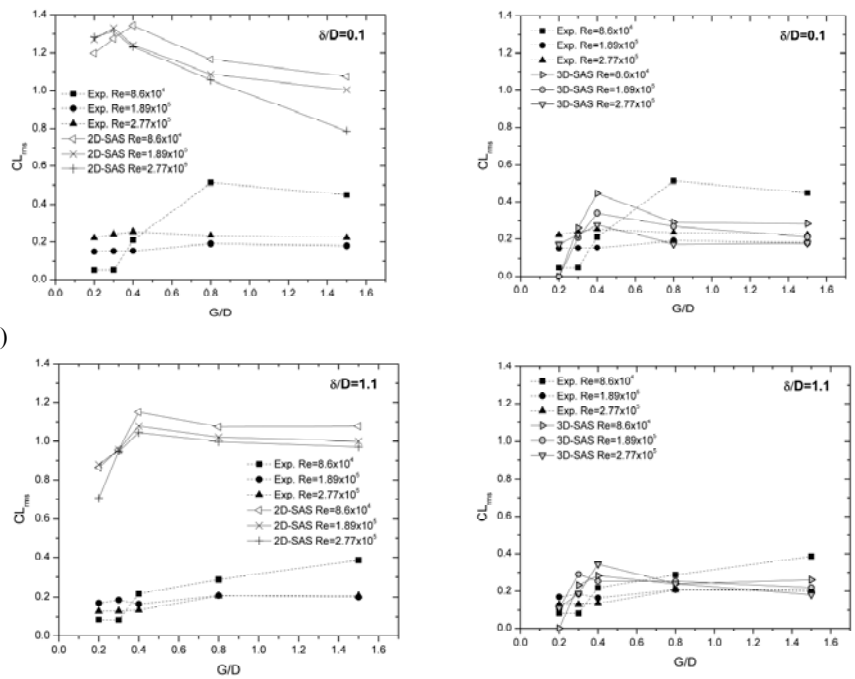

(a)

(b)

Fig. 12. RMS lift coefficient versus gap ratio; a) boundary layer thickness δ/D=0.1, b) boundary layer thickness δ/D=1.1.

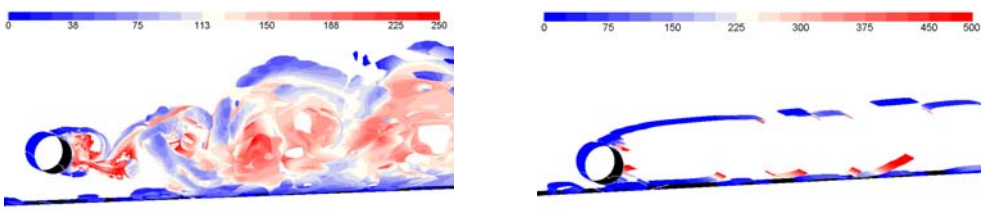

(a) (b)

Fig. 13. Iso-surfaces of instantaneous Q-criterion (Q=1[s^{-2}]) for Re=8.6x10^4 and δ/D=0.1 predicted by 3D-SAS; a) G/D=0.8; b) G/D=0.2.

4. CONCLUSIONS

Numerical investigations using Scale-Adaptive Simulation (SAS) turbulence model are carried out to study the flow around a circular cylinder near to a plane boundary at Reynolds numbers between $8.6x10^4$ and $2.77x10^5$ with two different boundary layer thicknesses (δ) on the plane boundary. Two and three-dimensional simulations are performed to examine the importance of the three-dimensionality of the flow. The effects of five different gap ratios (G/D) are investigated through the force coefficients, the Strouhal number, and the wake flow structures behind the cylinder. The main conclusions are as follows:

Regarding force coefficients, the drag and lift behavior predicted by the 2D and 3D-SAS simulations are in good agreement with experimental data. The mean forces, drag and lift, appeared to be strongly affected by the distance of the cylinder to the plane boundary. In addition, the C_D coefficient is dependent on the Reynolds number and it is influenced by the thickness of the boundary layer, while the C_L showed to be influenced by the thickness of the boundary layer but almost unaffected by the Re.

Regarding Strouhal number both 2D and 3D-SAS models over-predict the St value, however a similar trend is observed when compared with the experimental data. The Strouhal number results showed almost unaffected by the Re, by the thickness of the boundary layer and even unaffected by the value of the distance from the plane. An interesting observation to note is that the Strouhal number is very similar between 2D-SAS and 3D-SAS, suggesting that the frequency of vortex shedding is insensitive to the three-dimensional effects.

Regarding the vortex shedding and suppression clearly 3D-SAS performs better than 2D-SAS. In particular, the 3D-SAS predicted the critical value for suppression of vortex shedding ($G/D_{crit}=0.3$) which is in satisfactory agreement with experimental data for $Re=8.6x10^4$, whereas 2D-SAS simulation presented drawbacks to predict the critical gap ($G/D_{crit}=0.2$). In addition, for all Re the variations of C_{Lrms} with the gap ratio predicted, by 3D-SAS are in good agreement with experimental data, while 2D-SAS results over-predict them. Based on the numerical simulation results obtained by 3D-SAS, G/D_{crit} decreases when Re increases. On the other hand, despite G/D_{crit} decreases with the increase of δ for $Re=1.89x10^5$, there is no clear evidence that G/D_{crit} changes with the thickness of the boundary layer.

Based on the results presented in this paper, we conclude that the present SAS model is able to produce satisfactory numerical results for the problem of a cylinder near a plane. However, further investigations are required in order to perform a more detailed validation study of the SAS turbulence model for other type of flows.

ACKNOWLEDGEMENTS

This work has been partially supported by the Project PUE-IDIT, "Vulnerability of infrastructure and physical environment associated with fuel transportation and storage" financed by National Scientific and Technical Research Council (CONICET); and by the Project 06/B344, "Flows action in laminar structures by numerical methods" financed by National University of Cuyo. The first author has a Ph.D. fellowship from CONICET.

REFERENCES

Abrahamsen Prsic, M., Chen Ong, M., Pettersen, B. and Myrhaug, D. (2016). Large Eddy Simulations of flow around a circular cylinder close to a flat seabed, *Marine Structures* 46, 127-148.

Achenbach, E. (1971). Influence of surface roughness on the cross-flow around a circular cylinder, *Journal of Fluid Mechanics* 46, 321-335.

ANSYS Inc. (2014). Ansys Fluent 15 User's Guide.

ANSYS Inc. (2014). Ansys ICEM CFD 15 User's Guide.

Bearman, P. W. and M. M Zdravkovich (1978). Flow around a circular cylinder near a plane boundary, *Journal of Fluid Mechanics* 89, 33-47.

Buresti, G. and A. Lanciotti (1992). Mean and fluctuating forces on a circular cylinder in cross-flow near a plane surface, *Journal of Wind Engineering and Industrial Aerodynamics* 41, 639-650.

Deepakkumar, R., S. Jayavel and S. Tiwari (2017). Cross Flow past Circular Cylinder with Waviness in Confining Walls near the Cylinder, *Journal of Applied Fluid Mechanics* 10, 183-197.

Dipankar, A. and T. K. Sengupta (2005). Flow past a circular cylinder in the vicinity of a plane wall, *Journal of Fluids and Structures* 20, 403-423.

Göktuns, S. (1975). *The drag and lift characteristics of a cylinder placed near a plane surface*. M.Sc. thesis, Naval Postgraduate School, Monterey, California.

Lei, C., L. Cheng and K. Kavanagh (1999). Re-examination of the effect of a plane boundary on force and vortex shedding of a circular cylinder, *Journal of Wind Engineering Industrial Aerodynamics* 80, 263-286.

Lei, C., L. Cheng, S.W. Armfield and K. Kavanagh (2000). Vortex shedding suppression for flow over a circular cylinder near a plane boundary, *Ocean Engineering* 27, 1109-1127.

Menter F. R. (1994). Two-equation eddy viscosity turbulence models for engineering applications, *AIAA Journal* 32, 1598-1605.

Menter, F. R., M. Kuntz and R. Bender (2003). A scale-adaptive simulation model for turbulent flow predictions. *AIAA Paper 2003-0767, In: 41st AIAA Aerospace Sciences Meeting and Exhibit*, Reno, NV, USA.

Niemann, H. J. and N. Hölscher (1990). A review of recent experiments on the flow past circular cylinders, *Journal of Wind Engineering and Industrial Aerodynamics* 33, 197-209.

Nishino, T., G. T. Roberts and X. Zhang (2008). Unsteady RANS and detached-eddy simulations of flow around a circular cylinder in ground effect, *Journal of Fluids and Structures* 24, 18-33.

Nishino, T., G. T. Roberts and X. Zhang (2007). Vortex shedding from a circular cylinder near a moving ground, *Physics of Fluids* 19, 025103.

Ong, M. C., T. Utnes, L. E. Holmedal, D. Myrhaug and B. Pettersen (2008). Numerical simulation of flow around a marine pipeline close to the seabed, *Coastal Engineering* 3, 2730-2742.

Ong, M. C., T. Utnes, L. E. Holmedal, D. Myrhaug and B. Pettersen (2010). Numerical simulation of flow around a circular cylinder close to a flat seabed at high Reynolds numbers using a k- ε model, *Coastal Engineering* 57, 931-947.

Rajani, B. N., A. Kandasamy and S. Majumdar (2012). On the Reliability of Eddy Viscosity Based Turbulence Models in Predicting Turbulent Flow past a Circular Cylinder Using URANS Approach, *Journal of Applied Fluid Mechanics* 5, 67-79.

Shur, M. L., P. R. Spalart, M. K. Strelets and A. K. Travin (2002). Towards the Prediction of Noise from Jet Engines, *International Journal of heat and Fluid Flow* 24, 551-561.

Taniguchi, S. and K. Miyakoshi (1990). Fluctuating fluid forces acting on a circular cylinder and interference with a plane wall, *Experiments in Fluids* 9, 197-204.

Wang, X. K. and S. K. Tan (2008). Near-wake flow characteristics of circular cylinder close to a wall, *Journal of Fluids and Structures* 24, 605-627.